Electrical Conductivity Depth Modelling with a Multireceiver EMI Sensor for Prospecting Archaeological Features

TIMOTHY SAEY[1]*, **PHILIPPE DE SMEDT**[1], **EEF MEERSCHMAN**[1], **MOHAMMAD MONIRUL ISLAM**[1], **FUN MEEUWS**[1], **ELLEN VAN DE VIJVER**[1], **ALEXANDER LEHOUCK**[2,3] AND **MARC VAN MEIRVENNE**[1]

[1] *Research Group Soil Spatial Inventory Techniques, Faculty of Bioscience Engineering, Ghent University, Coupure 653, 9000 Gent, Belgium*
[2] *Abdijmuseum Ten Duinen 1138, Koninklijke Prinslaan 6-8, 8670 Koksijde, Belgium*
[3] *Department of Medieval History, Faculty of Arts Philosophy, Sint-Pietersnieuwstraat 35, 9000 Gent, Belgium*

ABSTRACT
Multiple apparent electrical conductivity (EC_a) measurements with an electromagnetic induction (EMI) sensor frequently reveal analogue patterns caused by conductive features in the soil. A procedure was proposed to highlight different archaeological anomalies based on combinations of the simultaneous EC_a measurements with the DUALEM-21S instrument. After selection of a 3.5 ha study site, 0.79 ha has been recorded by archaeological excavation. Since the majority of the archaeological features were found between the plough layer and 1.0 m below the soil surface, a set of four equations were developed to model the EC within that predefined depth interval. This set of four equations employed the four depth response curves specific to the four DUALEM-21S coil configurations. The modelled conductivity between 0.5 and 1.0 m (EC_2^*) showed a larger variability across the archaeological features than the raw EC data. To quantify the added value of this modelled conductivity, EC_2^* and measured EC_a were compared with the rasterized map of the archaeological traces. Finally, the EC_2^* map proved to be better able to distinguish between the archaeological features and the 'empty' background. This technique allowed the highlighting of vague anomalies in the simultaneous DUALEM-21S EC_a measurements. Copyright © 2011 John Wiley & Sons, Ltd.

Key words: DUALEM-21S; electromagnetic induction; medieval archaeology; EC-depth map; moated site; coastal plain

Introduction

Geophysical surveys have been providing archaeologists with effective solutions for the non-invasive exploration of archaeological sites. In most cases, these techniques are powerful means for the rapid and reliable detection of buried archaeological remains. The cost of these non-invasive investigations is obviously less than the cost of excavation of an entire archaeological site (Eppelbaum *et al.*, 2010).

Among geophysical methods, electromagnetic induction (EMI) is noteworthy as a tool in landscape archaeology and contextual site analysis. With EMI, areas of archaeological interest can be mapped with high lateral and vertical resolution to delineate feature densities of human and natural origin (see e.g. Simpson *et al.*, 2008; Rodrigues *et al.*, 2009). Consequently, EMI can in some cases be used as a reference to guide the planning of excavations and reduce the costs of exploration stages (Venter *et al.*, 2006; Forte and Pipan, 2008). Generally, EMI allows determining the electrical conductivity and magnetic susceptibility of soils from the observation of induced electromagnetic fields. The apparent electrical conductivity (EC_a) of the soil is the integration of the conductivities, or of the different entities, in the measured soil volume, while the apparent magnetic susceptibility (MS_a) integrates the magnetic soil properties of these different soil entities. Soil EC_a was initially determined to quantify the soil salinity (Slavich and Petterson, 1990). In non-saline conditions, differences in EC_a were attributed to variation in soil physical properties, such

* Correspondence to: T. Saey, Research Group Soil Spatial Inventory Techniques, Faculty of Bioscience Engineering, Ghent University, Coupure 653, 9000 Gent, Belgium. E-mail: Timothy.Saey@UGent.be

as particle size distribution, moisture content and organic matter (Carroll and Oliver, 2005). In archaeology, EMI instruments have been adopted from the 1960s onwards, with the introduction of 'soil conductivity meters' (Scollar, 1962; Gaffney and Gater, 2003). A more thorough understanding of the EMI signal and its spatial response allowed surveyors to gather straightforward and accurate information about changes in soil EC_a and MS_a (e.g. Tite and Mullins, 1970; Tabbagh, 1974; Parchas and Tabbagh, 1978) and to meet the demands of archaeologists (e.g. Tabbagh, 1986).

Today, the most commonly applied conductivity meter in archaeology is the EM38 (Geonics, Ltd), which allows measuring soil volumes down to 1.5 m beneath the surface (e.g. Lück and Eisenreich, 1999). Previously, several archaeological studies used EC_a with the EM38 instrument in the horizontal coplanar (HCP) dipole mode, with one transmitter and one receiver coil. Simpson *et al.* (2008) showed the EC_a maps to reveal the ditch of a moated site, a large channel (part of a marine tidal system) and large volumes of brick rubble and walls. Persson and Olofsson (2004) found a former excavation tunnel in their EC_a measurements. Lück *et al.* (2003) identified small structures such as posts or pits within their EC_a map and confirmed the potency for prospecting archaeological ditch systems. Moreover, EMI-derived conductivity survey was performed by a number of geoarchaeologists mapping palaeolandscapes (Bates and Bates, 2000; De Smedt *et al.*, 2011).

Starting from the 1990s, more information was gathered simultaneously by the application of multisensor, multipole or multi-electrode systems. Consequently, EMI instruments were developed to measure simultaneously EC_a and MS_a in different coil configurations. The use of several receivers to improve the depth of investigation and the horizontal discrimination of inhomogeneities was demonstrated by Simpson *et al.* (2009). Recently, the DUALEM-21S (Dualem Inc., Milton, Canada) was developed, which allows measuring both EC_a and MS_a at two coil orientations for two coil separations (Saey *et al.*, 2009).

Because of their specific spatial sensitivity, these multiple coil configurations have the potential to detect more archaeological features than individual measurements. For example, Simpson *et al.* (2009) showed that by subtracting two DUALEM-21S EC_a measurements, small anomalies can be revealed, whereas these can be masked by highly conductive soil features in single measurements. Despite this added vertical discrimination potential, EMI sensors with multiple coil configurations have been rarely used for archaeological prospecting.

Generally, EMI instruments are characterized by a continuous depth response function, determined by the instrument coil spacing and orientation. The measured EC_a is an integration of the conductivities (EC) of different features in the subsoil of a certain soil volume, determined by the depth sensitivity function of the EMI coil pair (McNeill, 1980). Based on this depth response function, the depth of exploration (DOE) can be defined as the depth at the 70% cumulative response. This implies that 30 % of the cumulative response comes from features below this DOE (Morris, 2009). Therefore, contrasting features with a large vertical extent (such as a clayey substrate) have a substantial contribution to the measured EC_a (Saey *et al.*, 2009), even if situated below the DOE. Most archaeological features, on the other hand, have a limited vertical depth extent, making them difficult to discern within one single EC_a measurement.

Therefore, our aim is to combine the four simultaneous EC_a measurements, obtained with the DUALEM-21S sensor, to focus on archaeological anomalies just below the ploughed topsoil. This technique should enable the archaeologist to recognize shallow archaeological features non-invasively. This vertical EC_a analysis of a multilayer EC_a dataset should enable archaeologists to better discriminate shallow archaeological features within predefined soil layers.

Site description

The study site is a 3.5 ha agricultural field and is a part of an 89 ha study area (Figure 1). The area was geophysically scanned to support archaeological excavations that were carried out before the construction of a golf course. The study site is located in the western part of the Belgian coastal plain (central coordinates: 51°06′46″N and 2°41′38″E; Figure 1) and is part of the former wetlands along the southern North Sea area, which stretch from Calais in northern France to Skagen in the north of Denmark.

This coastal plain is a polder area about 15–20 km wide with an extension in the western part of the plain along the River IJzer. The plain was created by embankment following post-glacial sea-level rise and is situated behind a belt of aeolian sand dunes (Baeteman, 1999, 2008; Baeteman and Declercq, 2002). Its particular microrelief results from both natural and human-induced processes. Sea-level fluctuations starting at the onset of the Holocene initiated peat formation and sediment accumulation behind the coastal barrier and caused the formation of tidal
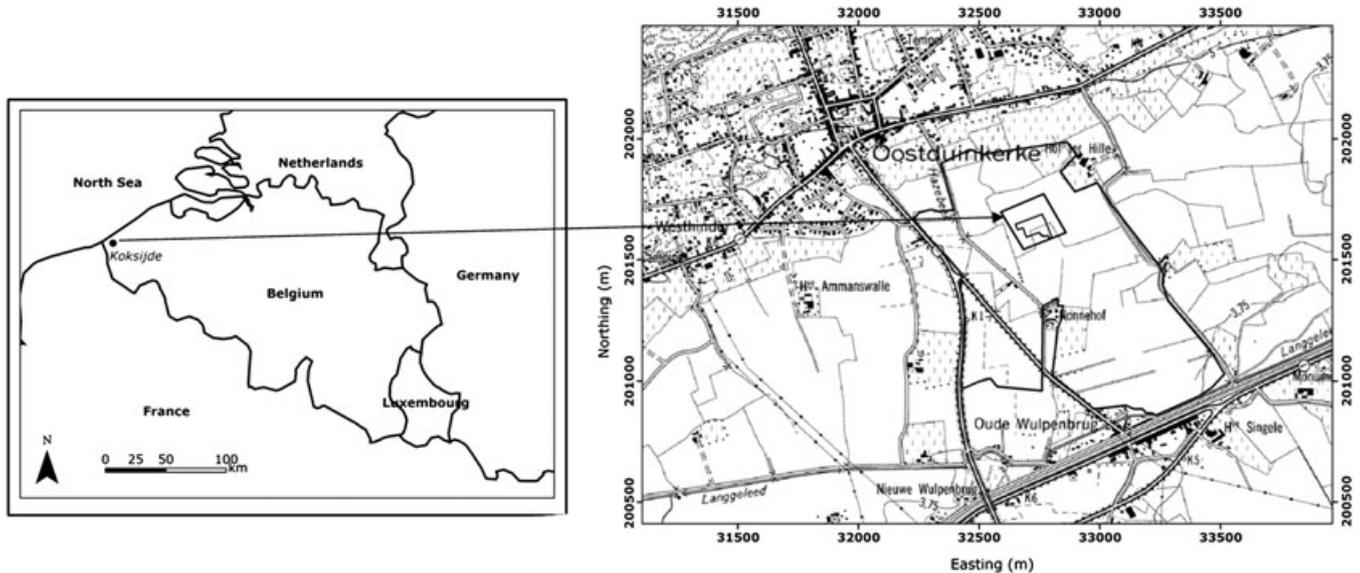
Figure 1. Location and topography of the study site in Belgium, indicating the boundaries of the golf course and the study and excavation sites (coordinates are according to the Belgian metric Lambert 72 projection).

channels in the peat layers and underlying sediments (Baeteman 1991, 2008; Ervynck *et al.*, 1999).

In the larger study area, which was part of the IJzer Estuary and palaeovalley, late Holocene sand and silt deposits dominate. Tidal channels were formed and filled in with sand deposits during the late *La Tène* and Roman period (from ca. 50 yr BC), with subsequent infilling with sand deposits starting in the fifth century AD. Finally, these channels were filled in with clayey sediments from the seventh century AD onwards (Baeteman, 2008).

Throughout the entire study area, soil characteristics are rather uniform and characterized by AC1C2 profiles, where the clayey, ploughed A-horizon overlies the clayey (C1) and sandy (C2) substrate.

Materials and methods

DUALEM-21S electromagnetic induction sensor

The DUALEM-21S electromagnetic induction sensor consists of one transmitter and four receiver coils at a fixed separation. The primary magnetic field is created by an alternating current passed through the transmitting coil. The magnetic component of this primary field creates eddy currents in the conductive soil below, which in turn induce their own secondary magnetic field. The induced secondary field is superimposed on the primary field and both create currents in the receiver coils, of which the resulting voltage and phase

are measured (McNeill, 1980). The ratio of the secondary over the primary field is proportional to the EC_a of the bulk soil in the quadrature-phase response. The four receiver coils of the DUALEM-21S instrument are located at spacings of 1, 1.1, 2 and 2.1 m from the transmitter. The 1 m and 2 m transmitter–receiver pairs are in a horizontal coplanar coil mode (1HCP and 2HCP), while the 1.1 m and 2.1 m pairs are placed in a perpendicular coil mode (1.1PERP and 2.1PERP). Both the transmitter–receiver spacing and the orientation of the coil determine the depth and response pattern of the signal and as such the DOE. This spatial sensitivity corresponding DOE can be described numerically by Maxwell's equations. McNeill (1980) approximated these by analytical equations defined by the cumulative response from the soil volume above a depth z (in m) for the horizontal coplanar dipole mode ($R_{HCP}(z)$). Dualem Inc. (2007) developed the equation of the cumulative response for the perpendicular dipole mode ($R_{PERP}(z)$) based on Wait (1962):

Table 1. Descriptive statistics of $EC_{a(1.1PERP)}$, $EC_{a(2.1PERP)}$, $EC_{a(1HCP)}$ and $EC_{a(2HCP)}$ for the 20,280 measurements on the 3.5 ha study site (in mS m^{-1} after conversion to a reference temperature of 25°C).

Variable	m	min	max	SD
$EC_{a(1.1PERP)}$	36	17	88	6
$EC_{a(2.1PERP)}$	42	28	71	6
$EC_{a(1HCP)}$	43	−6	67	5
$EC_{a(2HCP)}$	40	16	60	4

m, mean; min, minimum; max, maximum; SD, standard deviation.

$$R_{HCP}(z) = 1 - \left(4 \cdot \frac{z^2}{s^2} + 1 \right)^{-0.5} \tag{1}$$

$$R_{PERP}(z) = 2 \frac{z^2}{s^2} \left(4 \frac{z^2}{s^2} + 1 \right)^{-0.5} \tag{2}$$

with s being the transmitter–receiver spacing, and both $R_{HCP}(z)$ and $R_{PERP}(z)$ expressed as a percentage of the measured signal, relative to 1.

The DOE differs for the different coil configurations: 1.1PERP, 0.54 m; 2.1PERP, 1.03 m; 1HCP, 1.55 m; and 2HCP, 3.18 m (Saey *et al.*, 2009).

EC$_a$ survey

The EC$_a$ of the 3.5 ha study site was investigated with the DUALEM-21S proximal EMI soil sensor as a part of the investigation of the 85 ha golf course. The sensor was housed in a non-metal sled and pulled behind an all-terrain vehicle at a speed of about 6–10 km h^{-1} crossing the field along parallel lines 1.7 m apart. The
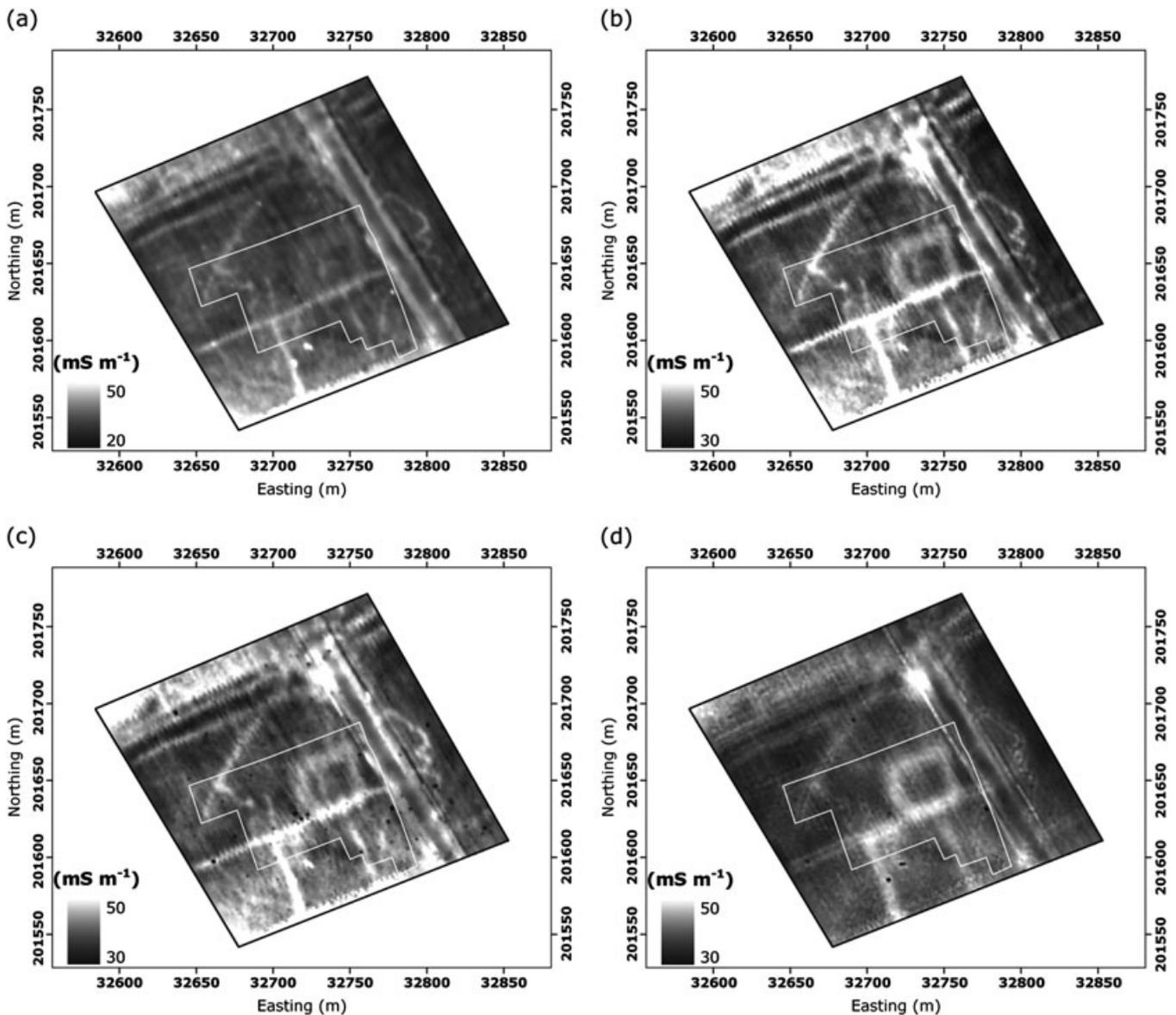

Figure 2. Measured apparent electrical conductivity map (converted to a reference temperature of 25°C) in (a) the 1.1 m perpendicular dipole mode (EC$_{a(1.1PERP)}$), (b) the 2.1 m perpendicular dipole mode (EC$_{a(2.1PERP)}$), (c) the 1 m horizontal coplanar dipole mode (EC$_{a(1HCP)}$) and (d) the 2 m horizontal coplanar dipole mode (EC$_{a(2HCP)}$), with the location of the excavated site (white line).

DUALEM-21S simultaneously measures four EC_a measurements that are recorded on a field computer. The computer was connected to a Trimble AgGPS332, in order to georeference the EC_a measurements with a pass-to-pass accuracy of approximately 0.10 m. Measurements of soil temperature at a depth of 70 cm allowed the conversion of the measurements to a reference temperature of 25°C. Using ordinary point kriging (Goovaerts, 1997), these field data were then interpolated to a 0.5 by 0.5 m grid.

EC-depth modelling

The four simultaneous EC_a measurements obtained with the DUALEM-21S sensor have their own depth sensitivity given by equations (1) and (2). In a layered soil build-up, the measured EC_a can be estimated by summing the conductivities (EC) and depth-weighted contributions of each delimited layer. Inversely, the EC of a defined layer can be determined based on the measured EC_a and the depth sensitivity curves. By establishing a set of four equations, the EC of three layers with predefined depth boundaries can be estimated accurately given the four measured EC_a values.

The aim was to transform the four EC_a measurements into three EC layers, representative of shallow (EC_1^*), medium (EC_2^*) and deep (EC_3^*) soil layers. Based on the characteristic depth response profiles for each coil configuration, the following four equations were formulated, taking the height of the DUALEM-21S sensor above the soil surface (Z_s) into account:

$$EC_{a(1.1PERP)} = \left[R_{PERP,1.1}(Z_1 + Z_s) - R_{PERP,1.1}(Z_s) \right] \cdot EC_1^*$$
$$+ \left[R_{PERP,1.1}(Z_2 + Z_s) - R_{PERP,1.1}(Z_1 + Z_s) \right] \cdot EC_2^*$$
$$+ \left[1 - R_{PERP,1.1}(Z_2 + Z_s) \cdot EC_3^* \right] \quad (3)$$

$$EC_{a(2.1PERP)} = \left[R_{PERP,2.1}(Z_1 + Z_s) - R_{PERP,2.1}(Z_s) \right] \cdot EC_1^*$$
$$+ \left[R_{PERP,2.1}(Z_2 + Z_s) - R_{PERP,2.1}(Z_1 + Z_s) \right] \cdot EC_2^*$$
$$+ \left[1 - R_{PERP,2.1}(Z_2 + Z_s) \cdot EC_3^* \right] \quad (4)$$

$$EC_{a(1HCP)} = \left[R_{HCP,1}(Z_1 + Z_s) - R_{HCP,1}(Z_s) \right] \cdot EC_1^*$$
$$+ \left[R_{HCP,1}(Z_2 + Z_s) - R_{HCP,1}(Z_1 + Z_s) \right] \cdot EC_2^*$$
$$+ \left[1 - R_{HCP,1}(Z_1 + Z_s) \cdot EC_3^* \right] \quad (5)$$

$$EC_{a(2HCP)} = \left[R_{HCP,2}(Z_1 + Z_s) - R_{HCP,2}(Z_s) \right] \cdot EC_1^*$$
$$+ \left[R_{HCP,2}(Z_2 + Z_s) - R_{HCP,2}(Z_1 + Z_s) \right] \cdot EC_2^*$$
$$+ \left[1 - R_{HCP,2}(Z_1 + Z_s) \cdot EC_3^* \right] \quad (6)$$

with $R_{PERPx}(z)$ and $R_{HCPx}(z)$ the cumulative responses above a depth z for the PERP and HCP mode and

transmitter–receiver coil spacing x. Z_1 represents the boundary between the first and second soil volume and Z_2 the interface of the second and third soil volume to be modelled. At each of the 20,280 measurement locations, this set of equations was solved to the unknown EC_1^*, EC_2^* and EC_3^* using the Levenberg–Marquardt algorithm (Marquardt, 1963).

Results and discussion

EC_a survey with the DUALEM-21S sensor

Table 1 summarizes the statistics of the four EC_a measurements taken with the DUALEM-21S sensor at 20,280 locations on the study site. The mean values of the EC_a increase with increasing DOE, but decrease from the 1HCP (DOE = 1.55 m) to the 2HCP (DOE = 3.18 m) coil configuration. This indicates an increasing soil conductivity of the measured soil volumes down to 1.55 m beneath the plough layer. The decrease in conductivity recorded with the 2HCP configuration suggests more resistive features between 1.55 and 3.18 m depth. The negative minimum value of $EC_{a(1HCP)}$ was caused by anomalies in the topsoil, such as small metal objects. Figure 2 shows the EC_a map of the study site. Here, different features of both anthropogenic and geological origin, were observed across the study site, primarily on the $EC_{a(1HCP)}$ and $EC_{a(2HCP)}$ measurements. The DUALEM-21S MS_a measurements do not depict the features of archaeological interest on this study site (not shown in this article). This is because the
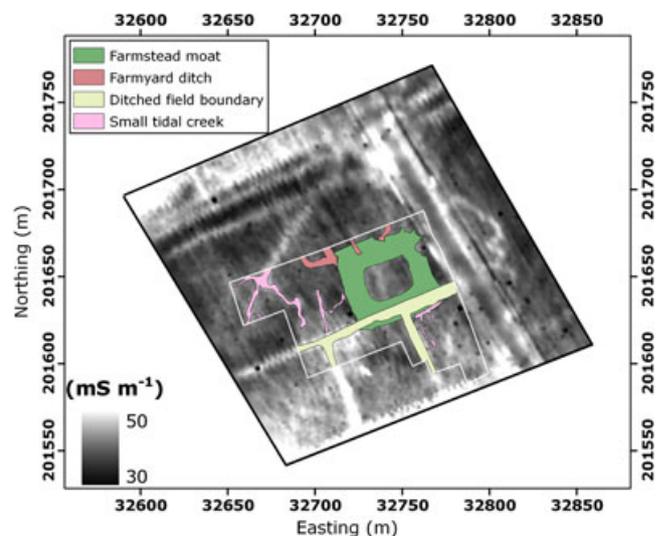

Figure 3. Measured apparent electrical conductivity map in the 1 m horizontal coplanar dipole mode ($EC_{a(1HCP)}$) with details of the excavated archaeological features. This figure is available in colour online at wileyonlinelibrary.com/journal/arp.

conductivity differences are obviously more distinct than the magnetic variation owing to the large textural variation across the study site. Therefore, we considered the conductivity results only as being representative for prospection of archaeological features.

Excavation results

Based on the EC_a data and complementary archaeological research, an area of 0.79 ha was excavated (white boundary on Figure 2). All excavated features were drawn and digitized (Figure 3). The excavation results confirmed the results of the EC_a survey by revealing the compacted clayey infilling of a medieval moat in the sandy subsoil. This farmstead moat, reaching to approximately 1 m below ground level, was infilled with compact greyish homogeneous silty to clayey material with embedded artefacts and charcoal fragments, similar to the infillings of the shallow and smaller farmyard ditch. The infill of a more recent (mid-twentieth century AD) ditched field boundary in the southern part of the excavation area was largely the same. However, here, a more organic infilling with reed and wood remains could be observed. Finally, the
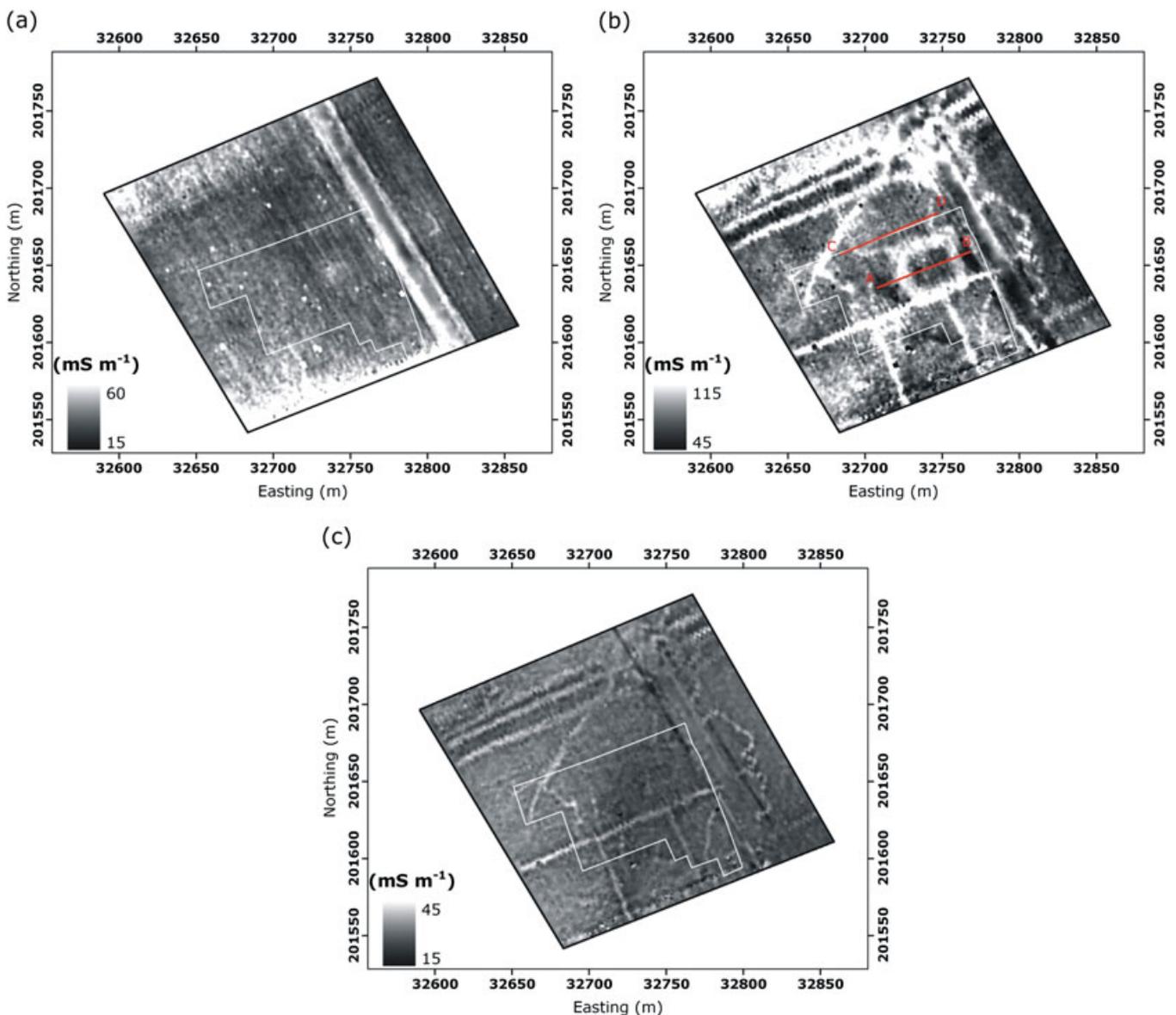

Figure 4. Modelled conductivity map between (a) 0 and 0.5 m (EC_1^*), (b) 0.5 and 1.0 m (EC_2^*) and (c) deeper than 1.0 m (EC_3^*).

small tidal creeks were infilled with homogeneous and very compact clayey sediment with numerous shell fragments.

Historical and archaeological interpretation

During the late Carolingian period (tenth century AD), the environment was well-developed into a cultural landscape (Lehouck *et al.*, 2011). According to this study, the medieval site, called *einzelhöfe*, was inhabited by a group of fishermen between the (late?) tenth and the twelfth century AD. The site formed part of scattered farmsteads of the fishing village of Oostduinkerke (some 800 m to the north), which probably developed along the southern bank of an old tidal branch of the River IJzer. This palaeotidal branch can be considered as the main tidal river of the area in that period (Lehouck, 2010).

The settlement was characterized by a bipartite structure of a residential upper court (area of the farmstead) and a non-residential lower farmyard. This kind of feature is typical for late medieval moated sites, but is not well documented for the earlier period. The site was discovered in 2008 by field surveying (microtopography, field walking and a coarse auger campaign); however, the bipartite structure was indistinguishable in the EC_a measurements.

EC-depth modelling

For the EC depth modelling, depth intervals were chosen based on the excavation results. As most of the archaeological features were located between 0.5 m and 1 m depth or just below the ploughed layer, we focused on modelling the EC between these depths.

The three maps are given in Figure 4. Layer EC_1^* (Figure 4a) shows that there is little variability in the topsoil (0–0.5 m). Layer EC_2^* (Figure 4b), on the other hand, amplifies the recorded archaeological features. In particular, the farmyard ditch becomes more pronounced compared with the four single EC_a measurements (Figure 2). The range of layer EC_2^* values is larger compared with the single EC_a ranges, resulting in more distinct differences between the archaeological traces (Figure 4b). In Figure 4c the farmstead moat and farmyard ditch disappear. The modelled EC_3^* layer reveals the existence of ditched field boundaries and small tidal creeks below a depth of 1 m.

Model evaluation

To complement the sensor measurements with field verifications we positioned two transects AB and CD

through both the farmstead moat and the farmyard ditches (Figure 4b). The EC_a and EC_2^* values along these transects are shown in Figure 5. When comparing the modelled EC_2^* with the EC_a measurements along both transects, EC_2^* shows a greater variability. To obtain a relative measure of the variability we calculated the coefficient of variation (CV), defined as the ratio between the standard deviation and the mean, along transects AB and CD. Along transect AB, crossing the farmstead moat, a clear distinction in the CV was observed: for EC_2^* a CV of 25% was found, whereas the CV of a single measurement varied between 6 and 8%.
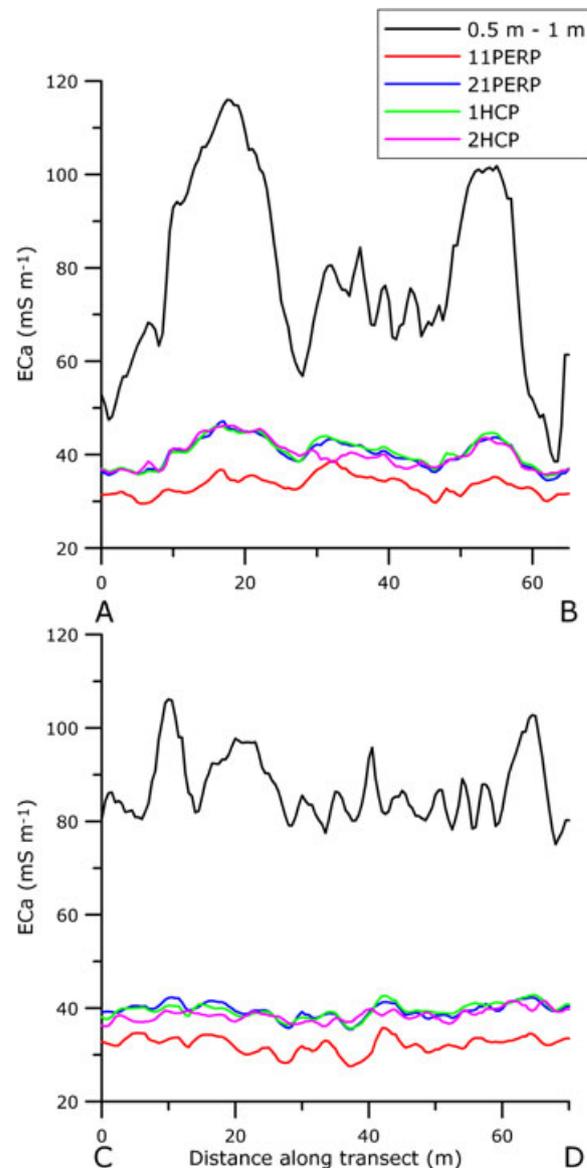

Figure 5. Measured apparent electrical conductivities (EC_a) and modelled conductivity between 0.5 and 1.0 m (EC_2^*) along transects AB and CD (Figure 4b). This figure is available in colour online at wileyonlinelibrary.com/journal/arp.
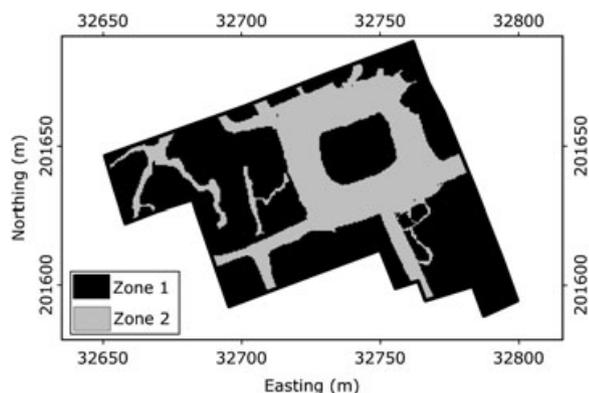
Figure 6. Rasterized map of the excavated archaeological features: zone 1, features absent; zone 2, features present.

Along transect CD the CV increases only slightly (8%) compared with the single EC_a measurements (3 – 5%), This was related to the less pronounced farmyard ditch underlying transect CD. These examples illustrate that the modelled EC_2^* exhibited a greater variability for archaeological features.

Both EC_a measurements and EC_2^* modelling were compared at the excavated site. $EC_{a(2.1PERP)}$ (Figure 2b) and $EC_{a(1HCP)}$ (Figure 2c) gave indications of the farmstead moat, ditched field boundaries and small tidal creeks, but the features became much better delineated on the EC_2^* map (Figure 4b). Moreover, the farmyard ditch could be localized on the EC_2^* map, and its boundary traced beyond the borders of the excavation area. The EC_a measurements and EC_2^* were evaluated using the rasterized validation image (Figure 6) from the excavated site. In Figure 6, zone 1 is where no shallow traces were found, whereas zone 2 represents the distinct archaeological features. Table 2 lists the mean and coefficient of variation of the EC_a measurements and the modelled EC_2^*, according to the two zones. The EC-depth modelling clearly

increased the EC_a variability within the zones, because EC_2^* records the highest CV values for both zones. In addition, EC_2^* shows less variation in zone 2, as would be expected because of the presence of archaeological features. The CV values for EC_a measurements, on the other hand, are the same for both zones, or are larger in zone 2. Moreover, the differences in mean values between the zones, indicated by the relative difference (RD), were greatest for EC_2^*, i.e. 20% for EC_2^* whereas the maximum RD for EC_a measurements was 8%. The RD was calculated as:

$$RD = \frac{X_{zone2} - X_{zone1}}{X_{zone2}} \qquad (7)$$

with X being the EC_2^* modelling or EC_a measurements.

Conclusions

Apparent electrical conductivity (EC_a) measured by multiple receivers of an EMI sensor increased the potential for detecting archaeological features when compared with a single-receiver EC_a survey. By using the multiple EC_a measurements to model EC values for predefined depth intervals (EC*), small measurement anomalies could be enhanced and information about the vertical extent of these features added. These resulting EC* models allowed a more accurate delineation of different types of archaeological features. This combination of multireceiver EMI sensors, combined with robust and straightforward depth modelling procedures, offers the potential to direct archaeological field surveys more efficiently as well as aid the spatial recognition of continuous patterns.

Acknowledgements

References

Baeteman C. 1991. Chronology of coastal plain development during the Holocene in West Belgium. *Quaternaire* **2**(3–4): 116–125. DOI: 10.3406/quate.1991.1960.

Table 2. Descriptive statistics of $EC_{a(1.1PERP)}$, $EC_{a(2.1PERP)}$, $EC_{a(1HCP)}$ and $EC_{a(2HCP)}$ measurements and modelled EC_2^* according to the two zones in Figure 6.

Variable	Zone 1		Zone 2		RD
	m	CV	m	CV	
$EC_{a(1.1PERP)}$	35	8	35	10	2
$EC_{a(2.1PERP)}$	41	8	44	10	7
$EC_{a(1HCP)}$	41	8	44	8	6
$EC_{a(2HCP)}$	40	7	43	7	8
EC_2^*	85	22	106	20	20

m, mean in mS m^{-1} after conversion to a reference temperature of 25°C; CV, coefficient of variation in %; RD, relative difference in %.

Baeteman C. 1999. The Holocene depositional history of the IJzer palaeovalley (Western Belgian coastal plain) with reference to the factors controlling the formation of intercalated peat beds. *Geologica Belgica* **2**(1–2): 39–72.

Baeteman C. 2008. Radiocarbon-dated sediment sequences from the Belgian coastal plain: testing the hypothesis of fluctuating or smooth late-Holocene relative sea-level rise. *The Holocene* **18**(8): 1219–1228. DOI: 10.1177/0959683608096597.

Baeteman C, Declercq P-Y. 2002. A synthesis of early and middle Holocene coastal changes in the western Belgian lowlands. *Belgeo* **2**: 77–107.

Bates MR, Bates CR. 2000. Multidisciplinary approaches to the geoarchaeological evaluation of deeply stratified sedimentary sequences: examples from Pleistocene and Holocene deposits in southern England, United Kingdom. *Journal of Archaeological Science* **27**(9): 845–858. DOI: 10.1006/jasc.2000.0584.

Carroll ZL, Oliver MA. 2005. Exploring the spatial relationships between soil physical properties and apparent electrical conductivity. *Geoderma* **128**(3–4): 354–374. DOI: 10.1016/j.geoderma.2005.03.008.

De Smedt P, Van Meirvenne M, Meerschman E, Saey T, Bats M, Court-Picon M, De Reu J, Zwertvaegher A, Antrop M, Bourgeois J, De Maeyer P, Finke PA, Verniers J, Crombe P. 2011. Reconstructing palaeochannel morphology with a mobile multicoil electromagnetic induction sensor. *Geomorphology* **130**(3–4): 136–141. DOI: 10.1016/j.geomorph.2011.03.009.

Dualem Inc. 2007. *DUALEM-21S User's Manual*. Dualem Inc.: Milton, Canada.

Eppelbaum LV, Khesin BE, Itkis SE. 2010. Archaeological geophysics in arid environments: Examples from Israel. *Journal of Arid Environments* **74**(7): 849–860. DOI: 10.1016/j.jaridenv.2009.04.018.

Ervynck A, Baeteman C, Demiddelde H, Hollevoet Y, Pieters M, Schelvis J, Tys D, Van Strydonck M, Verhaege F. 1999. Human occupation because of a regression, or the cause of a transgression? A critical review of the interaction between geological events and human occupation in the Belgian coastal plan during the first millenium AD. *Probleme der Küstenforschung im südlichen Nordseegebiet* **26**: 97–121.

Forte E, Pipan M. 2008. Integrated seismic tomography and ground-penetrating radar (GPR) for the high-resolution study of burial mounds (*tumuli*). *Journal of Archaeological Science* **35**(9): 2614–2623. DOI: 10.1016/j.jas.2008.04.024.

Gaffney C, Gater J. 2003. *Revealing the Buried Past: Geophysics for Archaeologists*. Tempus Publishing: Gloucestershire.

Goovaerts P. 1997. *Geostatistics for Natural Resources Evaluation*. Oxford University Press: New York.

Lehouck A. 2010. Het verdwenen landschap en de etymologie van Koksijde. Een landschapshistorische benadering op basis van plaatsnamen. In *Artikelen voor Magda Devos bij haar afscheid van de Universiteit Gent*, De Caluwe J, Van Keymeulen J (eds). Academia Press: Gent; 397–419.

Lehouck A, Eggermont N, Bracke M, Bradt T, Bruyninckx S, Wyns G, Acke B. 2011. Golf "Hof ter Hille" te Oostduinkerke-Wulpen : een stand van onderzoek 2009–2010 (Koksijde, W-Vl.). *Archaeologia Mediaevalis: Chronique – Kroniek – Chronik* **34**: 105–109.

Lück E, Eisenreich M. 1999. Geophysical prospection of archaeological sites in Brandenburg, Germany. *Archaeological Prospection* **6**(3): 125–133. DOI: 10.1002/(SICI)1099-0763(199909)6:3<125::AID-ARP111>3.0.CO;2-U.

Lück E, Callmer J, Skanberg T. 2003. The house of the Bailiff of Sövestad, Sweden – a multi-method geophysical case-study. *Archaeological Prospection* **10**(2): 143–151. DOI: 10.1002/arp.210.

Marquardt D. 1963. An algorithm for least-squares estimation of nonlinear parameters. *SIAM Journal on Applied Mathematics* **11**(2): 431–441. DOI: 10.1137/0111030.

McNeill JD. 1980. *Electromagnetic Terrain Conductivity Measurement at Low Induction Numbers*. Technical Note TN-6, Geonics Limited: Missisauga, Ontario.

Morris ER. 2009. Height-above-ground effects on penetration depth and response of electromagnetic induction soil conductivity meters. *Computers and Electronics in Agriculture* **68**(2): 150–156. DOI: 10.1016/j.compag.2009.05.009.

Parchas C, Tabbagh A. 1978. Simultaneous measurement of electrical conductivity and magnetic susceptibility of ground in electromagnetic prospecting. *Archaeo-Physika* **10**: 682–691.

Persson K, Olofsson B. 2004. Inside a mount: Applied geophysics in archaeological prospecting at the Kings' Mounds, Gamla Uppsala, Sweden. *Journal of Archaeological Science* **31**(5): 551–562. DOI: 10.1016/j.jas.2003.10.003.

Rodrigues SI, Porsani JL, Santos VRN, DeBlasis PAD, Giannini PCF. 2009. GPR and inductive electromagnetic surveys applied in three coastal sambaqui (shell mounds) archaeological sites in Santa Catarina state, South Brazil. *Journal of Archaeological Science* **36**(10): 2081–2088. DOI: 10.1016/j.jas.2009.05.013.

Saey T, Simpson D, Vermeersch H, Cockx L, Van Meirvenne M. 2009. Comparing the EM38DD and DUALEM-21S sensors for depth-to-clay mapping. *Soil Science Society of America Journal* **73**(1): 7–12. DOI: 10.2136/sssaj2008.0079.

Scollar I. 1962. Electromagnetic prospecting methods in archaeology. *Archaeometry* **5**(1): 146–153. DOI: 10.1111/j.1475–4754.1962.tb00566.x.

Slavich PG, Petterson GH. 1990. Estimating average rootzone salinity for electromagnetic (EM-38) measurements. *Australian Journal of Soil Research* **28**(3): 453–463. DOI: 10.1071/SR9900453.

Simpson D, Lehouck A, Van Meirvenne M, Bourgeois J, Thoen E, Vervloet J. 2008. Geoarchaeological prospection of a medieval manor in the Dutch polders using an electromagnetic induction sensor in combination with soil augerings. *Geoarchaeology* **23**(2): 305–319. DOI: 10.1002/gea.20214.

Simpson D, Van Meirvenne M, Saey T, Vermeersch H, Bourgeois J, Lehouck A, Cockx L, Vitharana UWA. 2009. Evaluating the multiple coil configurations of the EM38DD and DUALEM-21S sensors to detect archaeological anomalies. *Archaeological Prospection* **16**(2): 91–102. DOI: 10.1002/arp.349.

Tabbagh A. 1974. Définition des caractéristiques d'un appareil électromagnétique classique adapté à la prospection archéologique. *Prospezioni Archeologiche* **9**: 21–33.

Tabbagh A. 1986. What is the best coil orientation in the Slingram electromagnetic prospecting method? *Archaeometry* **28**(2): 195–196. DOI: 10.1111/j.1475–4754.1986.tb00386.x.

Tite MS, Mullins C. 1970. Electromagnetic prospecting on archaeological sites using a soil conductivity meter. *Archaeometry* **12**(1): 97–104. DOI: 10.1111/j.1475–4754.1970.tb00010.x.

Venter ML, Thompson VD, Reynolds MD, Waggoner Jr JC. 2006. Integrating shallow geophysical survey: archaeological investigations at Totógal in the Sierra de los Tuxtlas, Veracruz, México. *Journal of Archaeological Science* **33**(6): 767–777. DOI: 10.1016/j.jas.2005.10.008.

Wait JR. 1962. A note on the electromagnetic response of a stratified earth. *Geophysics* **27**(3): 382–385. DOI: 10.1190/1.1439028.